$M(PPh_3)_2(Cl_4Q)Cl_2$ (M = Ru, Os) complexes are more difficult to assign. Redox processes of the tetrachloroquinone ligand occur at potentials that are approximately 0.5 V more positive than the corresponding potentials of the DBQ ligand.[12] The first reduction of $Os(PPh_3)_2(Cl_4Q)Cl_2$ shows the shift relative to its Ru analogue, which may be characteristic of a M(III)/M(II) couple. Yet the reductions of both the Ru and Os complexes are shifted positively relative to those of their DBQ analogues in a way that would suggest that they are quinone ligand-based. Similar ambiguities existed in the assignment of couples of the $[M(bpy)_2(Q)]^+$ (M = Ru, Os; Q = DBCat, Cat, Cl_4Cat) series.[7] The problem may be understood by recognizing that the electronic levels responsible for electrochemical activity represent combinations of metal and quinone ligand orbital contributions. The shift from Ru to Os or from DBQ to ClQ may result in changes in orbital composition that give rise to apparently irrational shifts in electrochemical potentials. The conclusion from this characterization is that metal–quinone delocalization contributes to the electronic structure of the $M(PPh_3)_2(Q)Cl_2$ redox series in much the same way that it appeared for the $M(bpy)_2(Q)$ series.

Structural characterization on $Os(PPh_3)_2(DBQ)_2$ shows that the trend toward shorter M–O bond lengths and longer ligand C–O lengths found for the $ML_4(Q)$ and $M(Q)_3$ series of Ru and Os complexes is carried over to the $M(PPh_3)_2(Q)_2$ series. The complex in the solid state appears to be a bis(catecholate) complex of Os(IV) while structural characterization of $Ru(PPh_3)_2(Cl_4SQ)_2$ showed ligand structural features that were typically semiquinone.[8] Spectral and electrochemical similarities between corresponding members of the series $Ru(bpy)(Q)_2$ and $Ru(PPh_3)_2(Q)_2$ series led to the conclusion that the electronic levels associated with these properties were insensitive to metal orbital energy and that, in solution, the electronic structure of these complexes was the result of interligand delocalization.[8] Comparison of the corresponding members of M $Os(PPh_3)_2(Q)_2$ series with M = Ru and Os offers the opportunity to extend this investigation. Spectra listed in Table V and shown in Figure 6 bear close resemblance, particularly in the visible and near-infrared regions, to spectra of corresponding Ru complexes. Electrochemical potentials listed in Table VI show the same progressive shift in the positive direction from $Os(PPh_3)_2(DBQ)_2$ to the mixed-ligand complex, $Os(PPh_3)_2(DBQ)(Cl_4Q)$, and to $Os(PPh_3)_2(Cl_4Q)_2$. Further, the information in Table VI shows the close correspondence between related couples for the Ru and Os complexes. This observation serves to reinforce the view that metal orbital contributions to the frontier orbital structure of the $M(PPh_3)_2(Q)_2$ (M = Ru, Os) and $Ru(bpy)(Q)_2$ series are quite small. A more detailed comparison of these effects will be presented once studies on the $Os(bpy)(Q)_2$ series are complete.

Acknowledgment. This research was supported by the National Science Foundation under Grant CHE 88-09923. Ruthenium trichloride was provided by Johnson Matthey, Inc. through their Metal Loan Program.

Supplementary Material Available: For $Os(PPh_3)_2(DBQ)Cl_2$ and $Os(PPh_3)_2(DBQ)_2$, tables giving crystal data and details of the structure determination, atom coordinates, bond distances and angles, anisotropic thermal parameters, and hydrogen atom locations (26 pages); listings of observed and calculated structure factors for both compounds (33 pages). Ordering information is given on any current masthead page.

Contribution from the Departments of Chemistry, Montana State University, Bozeman, Montana 59717, and Western New Mexico University, Silver City, New Mexico 88061

Vitamin B_6 Model Reactions. 4. Stereoelectronic Catalysis of Carbon–Hydrogen Bond-Breaking Reactions and Crystal and Molecular Structure of Tetramethylammonium Bis(pyridoxylideneglycinato)cobaltate(III)–4.5-Water

Andrew G. Sykes,† Raymond D. Larsen,† James R. Fischer,‡ and Edwin H. Abbott*,†

Received July 18, 1990

The anionic complex bis(pyridoxylideneglycinato)cobaltate(III) holds the pyridoxal (vitamin B_6) Schiff base of glycine in a fixed conformation. Rates of carbon–hydrogen bond breaking have been measured for the diastereotopic protons of the glycine moiety's methylene group. Nuclear magnetic resonance measurements show that the fastest exchange occurs for the proton whose C–H bond is more nearly dihedrally perpendicular to the plane of the π system in the aromatic ring. Activation parameters are reported, and $\Delta H^{\ddagger}$ is found to be reduced for the more rapidly exchanging proton. The structure of the anion was determined by the X-ray crystallography of its tetramethylammonium salt, providing further insight into the factors responsible for the differential reactivity of the methylene protons. Crystallographic data are as follows: $P\bar{1}$, a = 8.545 (5) Å, b = 12.761 (6) Å, c = 14.158 (8) Å, α = 98.85 (4)°, β = 94.95 (5)°, γ = 91.08 (4) Å, V = 1519 (1) Å^3, Z = 2 (R = 0.090, R_w = 0.088).

Introduction

Vitamin B_6, in one of its forms, is the heterocyclic aldehyde pyridoxal (I). It is an essential cofactor to a large number of enzymes that catalyze many diverse reactions of amino acids.[1]

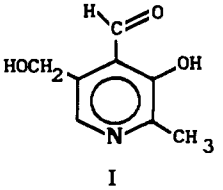

I

These reactions are known to proceed through Schiff base formation at the enzyme active site and are simply formulated as proceeding through Snell–Braunstein electron shifts into the pyridine ring as indicated in II. Accordingly, reactions are

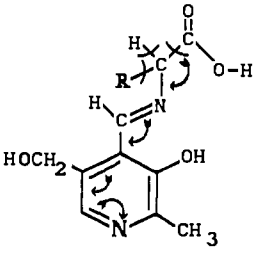

II

formulated as beginning by breaking one of the three bonds to the amino acid α-carbon atom. Some years ago, Dunathan hypothesized that the enzyme could select the bond to be broken

† Montana State University.
‡ Western New Mexico University.

(1) (a) Metzler, D. E.; Ikawa, M.; Snell, E. E. *J. Am. Chem. Soc.* **1954**, *76*, 648. (b) Martell, A. E. *Adv. Enzymol. Relat. Areas Mol. Biol.* **1982**, *53*, 163.

0020-1669/91/1330-2911$02.50/0

by causing a rotation about the amino acid α-carbon-to-nitrogen bond so that the electrons bonding this group could most easily flow into the π system of the azomethine group and the aromatic ring.[2] This rotation would place the group dihedrally perpendicular (orthogonal) to the plane of the aromatic–imine π system. He also pointed out that such an orientation could be significant in the enhancement of reaction rate brought about by the enzyme.

We have been interested in evaluating the catalytic enhancements that can be brought about by orienting the amino acid α-carbon substituents properly in model systems. To this end, we synthesized the bis(pyridoxylideneglycinato)cobaltate(III) anion.[3] In this complex two Schiff bases are expected to be bound to the cobalt(III) as indicated in III. A preliminary NMR study

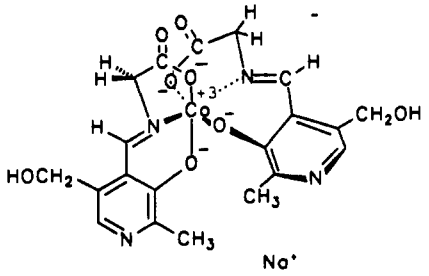

III

at 100 MHz showed that deuterium exchange at the glycine methylene group was biphasic. We studied the rates and activation parameters of this process and found one of the proton-exchange reactions to be much faster than the other. Its activation enthalpy was significantly reduced as well, suggesting that important reaction rate enhancement processes might be at work. It had been necessary to work at high concentrations. One undesirable consequence was that the rate of the reaction was bimolecular in complex, suggesting that the pyridine nitrogen of a second complex was functioning as the base in the proton-exchange reactions of the complex. Herein we report the kinetics of these proton-exchange reactions carried out under better controlled conditions. We also report the detailed molecular structure of the complex and identify structural features that may be responsible for the different rates of carbon–hydrogen bond breaking observed at the glycine methylene group in this complex.

Experimental Section

I. Syntheses. a. Sodium Bis(pyridoxylideneglycinato)cobaltate(II). Glycine (0.75 g, 10.0 mmol) and sodium hydroxide (0.80 g, 20.0 mmol) were dissolved in 100 mL of absolute methanol. Pyridoxal hydrochloride (2.04 g, 10.0 mmol) was added, and the mixture was stirred for 30 min. Cobalt(II) chloride hexahydrate (1.19 g, 5.0 mmol) dissolved in 15 mL of methanol was added dropwise with vigorous stirring. The solution was stirred for 15 min and then placed in an ice bath for 4 h. The brown solid product was filtered off and dried in vacuo overnight. Yield: 55%. The volume of methanol noted, ca. 115 mL, will hold the byproduct sodium chloride in solution.

b. Sodium Bis(pyridoxylideneglycinato)cobaltate(III). Three millimoles (1.5 g) of the cobalt(II) complex was dissolved in 150 mL of absolute methanol with 1.5 mL of 2 M sodium hydroxide (3 mmol). The solution was heated to 50 °C, and undissolved solids were removed by filtration. Activated charcoal (0.75 g, Darco G-60, Sargent-Welch) was added, and the solution was aerated for 3 h by drawing air through a gas dispersion frit while in an ice bath. The charcoal was then removed by filtration. The filtrate was rotovapped and then dried in vacuo to give a dark brown product. Anal. Calcd for $NaCoC_{20}H_{20}N_4O_8 \cdot 1.5H_2O$: C, 43.43; H, 4.16. Found: C, 43.83; H, 4.36. ^1H NMR in water-d_2 (δ referenced to HMDS capillary): 1.548 (s, 2-CH_3), 4.858 (s, 5-CH_2), 5.166 (AB, glycyl CH_2 mean value), 7.641 (s, 6-H), 9.017 (s, azomethine CH).

c. Purification of the Co(III) Complex. Solid samples of the Co(III) complex decompose slowly to form traces of paramagnetic Co(II), which broaden NMR resonances and make further purification desirable just prior to kinetic runs. Typically, 0.7 g of the Co(III) complex was dissolved in 7 mL of distilled water, and the solution was extracted three times with 1.5 mL of 0.05 M 8-hydroxyquinoline (oxine) in chloroform. The aqueous phase was extracted four times with 1.5-mL portions of chloroform or was extracted until the organic phase remained colorless. The purified complex was rotovapped and dried in vacuo. Yield: 80%.

II. Hydrogen–Deuterium Exchange Reactions. Reactions were run in water-d_2 carbonate/bicarbonate buffers (0.01 M total carbonate) with 0.8 M potassium chloride present to maintain ionic strength. Typically, 1.3 mg of the complex was dissolved in 0.6 mL of buffer for a kinetic run. The pH of the solution was measured at the end of each run by using a glass electrode and a Brinkmann E512 pH meter. pDs were calculated as pD = pH + 0.41.[4] $[OD^-]$ was calculated[5] as $[OD^-] = 1.35 \times 10^{-15}/[D^+]$. Kinetic measurements were carried out with a Bruker WM-250 NMR spectrometer operating at 250 MHz. The exchange reaction was measured by loss of NMR proton signal for the glycyl protons, which are nonequivalent in this molecule. The pyridoxal 5-CH_2 resonance was used as an internal reference, as it did not change in peak area during the time of the kinetic runs. The A and B wings of the glycyl AB multiplet are well resolved at 5.4 T and were integrated separately. The pseudo-first-order reaction rates, psi, were determined from the slopes of plots of ln [H] vs time. Second-order deuterioxide-dependent reaction rate constants were calculated as k = psi/$[OD^-]$ after verifying that reactions were first order in $[OD^-]$.

III. Structure Determination and Refinement: Tetramethylammonium Bis(pyridoxylideneglycinato)cobaltate(III)–4.5-Water. Crystals were grown by vapor diffusion of acetone into an aqueous solution of the sodium salt of the complex and tetramethylammonium chloride. A plate-shaped dark brown crystal (approximately 0.05 × 0.70 × 0.70 mm) was mounted on a glass fiber for crystallographic data collection. The crystal was coated with a 3:1 mixture of Paratone-N and mineral oil to retard the loss of lattice water. Unit cell dimensions were obtained by least-squares refinement using 21 centered reflections for which 17° < 2θ < 22° (graphite-monochromatized Mo Kα radiation). Axial photographs showed triclinic symmetry, and the centrosymmetric space group, suggested by the unit cell volume, was used for structure solution and initial refinement. Reflections exhibited rather broad θ/2θ profiles (2.2–2.5°) and even broader and varied ω profiles, indicating either an undesirably high degree of mosaicity or inclusion of water layers within the crystal or both. The crystal was used for data collection, in spite of its poor quality, because single crystals were extremely difficult to obtain, and repeated attempts by many methods over a year's time failed to produce crystals of better quality. Intensity data were taken on a Nicolet R3mE four-circle diffractometer. Three check reflections, monitored every 100 reflections, showed approximately 20% loss of intensity during the course of data collection, and the intensity data were scaled accordingly. Crystallographic data are given in Table I.

Table I. Crystallographic Data for Tetramethylammonium Bis(pyridoxylideneglycinato)cobaltate(III)–4.5-Water

$[N(CH_3)_4][Co(C_{10}H_{10}N_2O_4)_2] \cdot 4.5H_2O$	fw = 658.63
a = 8.545 (5) Å	space group $P\bar{1}$ (No. 2)
b = 12.761 (6) Å	T = 24 °C
c = 14.158 (8) Å	λ = 0.71069 Å (Mo Kα)
α = 98.85 (4)°	ρ_{calcd} = 1.44 g cm^{-3}
β = 94.95 (5)°	μ = 6.3 cm^{-1} (Mo Kα)
γ = 91.08 (4)°	transm coeff = 0.75–0.98
V = 1519 (1) Å^3	$R(F_o)$ = 0.090
Z = 2	$R_w(F_o)$ = 0.088

Data reduction,[6] including corrections for Lorentz and polarization effects, gave 8885 independent reflections in the range 4° < 2θ < 60°, of which 2437 with $I > 2.5\sigma(I)$ were used for structure refinement. The cobalt position was determined from a Patterson synthesis, and the remaining non-hydrogen positions of the cobalt complex and the tetramethylammonium ion were located by difference syntheses. Difference maps also revealed at least eight possible water sites in the lattice, of which only one appeared to be fully occupied. Some combinations of the other seven sites were mutually excluded from full occupancy by unreasonably short oxygen–oxygen separations, and all seven were involved in one or more mutually exclusive pairings. The apparent partial occupancy of water sites, together with a rather high R value, prompted reconsideration of the choice of the centrosymmetric space group. A difference

(2) Dunathan, H. C. *Proc. Natl. Acad. Sci. U.S.A.* **1966**, *55*, 712.
(3) Fischer, J. R.; Abbott, E. H. *J. Am. Chem. Soc.* **1979**, *101*, 2781.
(4) Covington, A. K.; Paabo, M.; Robinson, R. A.; Bates, R. J. *Anal. Chem.* **1968**, *40*, 700–706.
(5) Technical Note 400, National Bureau of Standards, as cited in: *The CRC Handbook of Chemistry and Physics*, 61st ed.; CRC Press: Boca Raton, FL, 1980; p D168.
(6) All crystallographic calculations were performed on a Data General Eclipse computer using a SHELXTL program package by G. M. Sheldrick, Nicolet Instrument Corp., Madison, WI.

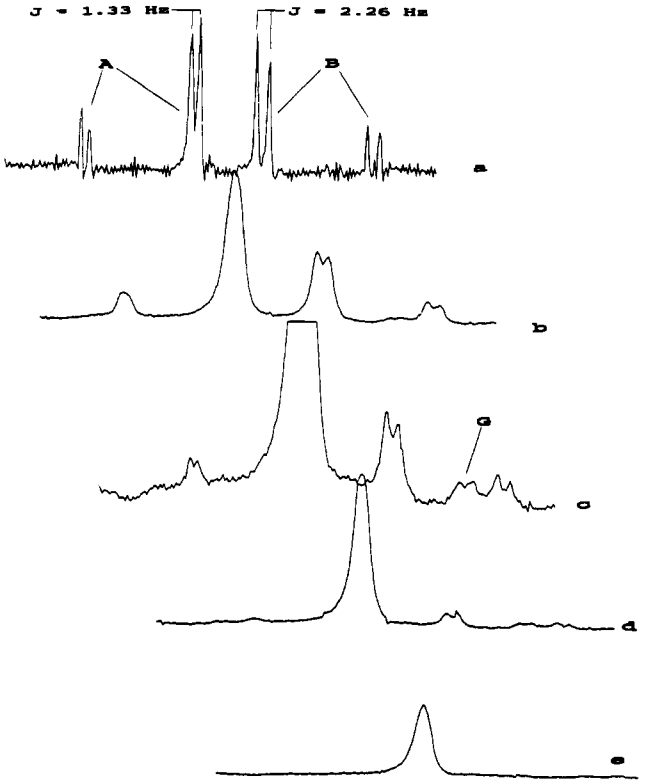

Figure 1. Changes in the proton spectrum of the glycine methylene AB pattern as deuterium exchange occurs in the bis(pyridoxylideneglycinato)cobaltate(III) anion. Spectrum a has been Gaussian-multiplied for resonance enhancement. The four-bond pseudoallylic coupling to the azomethine proton is indicated on the primary resonances. Spectrum c is amplified to show the intermediate geminal HD glycyl compound, marked G. The downfield proton has been replaced by a deuterium. Spectrum e was taken during the concluding phase of the reaction when the more rapidly exchanging upfield proton had fully exchanged.

map calculated for the alternative space group, $P1$, and phased by the cobalt positions showed inversion symmetry for the light-atom peaks with the inversion center midway between the cobalt sites. Attempts to refine the structure in $P1$ did not converge and gave unreasonable bond distances and substantially higher R values. These results confirmed the correctness of the initial assignment of space group $P\bar{1}$. The structure was refined by block-cascade least squares, minimizing $\sum w\Delta^2$ with 101 parameters defined in each full-matrix block. Absorption corrections were calculated by Gaussian integration using measured crystal dimensions between indexed crystal faces. Atomic scattering factors, including terms for anomalous scattering, were taken from ref 7.

Anisotropic thermal parameters were used for all non-hydrogen atoms except those of the lattice waters. One of these was presumed to be fully occupied and was refined with anisotropic thermal parameters. The others were initially assigned the equivalent isotropic temperature factor of the oxygen atom at the fully occupied site. During successive cycles of refinement, the isotropic thermal parameters and site occupancy factors for the partially occupied water positions were alternately refined. The site occupancy factors refined to values that were consistent with the mutually exclusive pairings of water sites indicated by oxygen–oxygen distances. During the final cycles of refinement, site occupancy factors were constrained such that their sums for mutually exclusive pairs of water sites could not exceed unity. This structure refinement model indicated a total of approximately 4.5 lattice water molecules per cobalt complex. Refinement of the thermal parameters of the tetramethylammonium carbon atoms indicated significant disorder of the ion around the relatively localized nitrogen atom position. The limited number of observed data precluded any attempt to model this disorder. The weighting scheme used was $w = k(\sigma^2(F_o) + 0.003F_o^2)^{-1}$. No corrections for extinction were needed. Except for those of methyl groups and water molecules, reasonable hydrogen positions were identified on difference maps. Hydrogens for the lattice waters and the tetramethylammonium ion were not included in the structure refinement. Calculated positions were used for all other hydrogens, except the hydroxyl hydrogen positions, which were refined with the constraint that the O–H distances for both groups be the same (refined to 0.8 (1) Å). A common refined isotropic thermal parameter was used for all hydrogens (refined to 0.078 (9) Å^2). The structure was refined to a final R value of 0.090, which is typical for similar compounds that exhibit rather poor crystal quality and disordered lattice water molecules.[8-10] Except for the usual ripple near the cobalt position, the largest peaks on the final difference map (0.44 e/Å^3) were located near the lattice water sites and could be interpreted as either hydrogen positions or additional partially occupied water oxygen positions. Atom coordinates are given in Table II.

Table II. Atom Coordinates and Equivalent Isotropic Temperature Factors (Å^2) with Standard Deviations in Parentheses for $[N(CH_3)_4][Co(C_{10}H_{10}N_2O_4)_2]\cdot 4.5H_2O$

	x/a	y/b	z/c	U_{eq}[a]
Co	0.2365 (2)	0.2317 (1)	0.3812 (1)	0.030 (1)
C(2a)	0.489 (1)	0.3318 (7)	0.634 (1)	0.035 (4)
C(3a)	0.410 (1)	0.3990 (7)	0.546 (1)	0.028 (4)
C(4a)	0.340 (1)	0.4365 (7)	0.535 (1)	0.030 (4)
C(5a)	0.353 (1)	0.5205 (7)	0.614 (1)	0.036 (4)
C(6a)	0.433 (1)	0.504 (1)	0.696 (1)	0.039 (4)
C(2'a)	0.566 (1)	0.230 (1)	0.650 (1)	0.058 (5)
C(4'a)	0.264 (1)	0.4537 (7)	0.445 (1)	0.034 (4)
C(5'a)	0.276 (1)	0.627 (1)	0.607 (1)	0.051 (5)
C(7a)	0.145 (1)	0.3968 (7)	0.284 (1)	0.043 (4)
C(8a)	0.042 (1)	0.296 (1)	0.243 (1)	0.047 (4)
N(1a)	0.504 (1)	0.4135 (7)	0.7080 (7)	0.048 (4)
N(2a)	0.221 (1)	0.3780 (6)	0.3746 (7)	0.034 (3)
O(1a)	0.406 (1)	0.2558 (5)	0.4791 (5)	0.032 (2)
O(2a)	0.066 (1)	0.2144 (5)	0.2829 (5)	0.041 (3)
O(3a)	−0.056 (1)	0.3001 (6)	0.1751 (6)	0.068 (4)
O(4a)	0.115 (1)	0.6054 (5)	0.5799 (7)	0.049 (3)
C(2b)	0.055 (1)	0.2167 (7)	0.634 (1)	0.039 (4)
C(3b)	0.111 (1)	0.1795 (7)	0.545 (1)	0.033 (4)
C(4b)	0.173 (1)	0.0768 (7)	0.531 (1)	0.029 (4)
C(5b)	0.180 (1)	0.0173 (7)	0.608 (1)	0.033 (4)
C(6b)	0.122 (1)	0.062 (1)	0.691 (1)	0.043 (4)
C(2'b)	−0.007 (1)	0.328 (1)	0.654 (1)	0.058 (5)
C(4'b)	0.222 (1)	0.0313 (7)	0.442 (1)	0.034 (4)
C(5'b)	0.248 (1)	−0.0897 (7)	0.602 (1)	0.043 (4)
C(7b)	0.298 (1)	0.037 (1)	0.281 (1)	0.043 (4)
C(8b)	0.394 (1)	0.118 (1)	0.241 (1)	0.042 (4)
N(1b)	0.056 (1)	0.1587 (7)	0.7060 (7)	0.045 (4)
N(2b)	0.245 (1)	0.0838 (6)	0.3733 (6)	0.030 (3)
O(1b)	0.095 (1)	0.2403 (5)	0.4768 (5)	0.036 (3)
O(2b)	0.380 (1)	0.2149 (5)	0.2830 (5)	0.040 (3)
O(3b)	0.477 (1)	0.0913 (6)	0.1781 (6)	0.066 (4)
O(4b)	0.407 (1)	−0.0790 (5)	0.5800 (5)	0.048 (3)
N(3)	0.378 (2)	0.245 (1)	−0.029 (1)	0.095 (6)
C(11)	0.496 (4)	0.308 (2)	0.045 (2)	0.18 (1)
C(12)	0.336 (3)	0.304 (2)	−0.108 (1)	0.13 (1)
C(13)	0.445 (4)	0.141 (2)	−0.066 (2)	0.19 (2)
C(14)	0.235 (3)	0.226 (3)	0.018 (2)	0.21 (2)
O(5w)	0.871 (1)	0.216 (1)	0.864 (1)	0.108 (5)
O(6w)[b]	0.781 (2)	0.102 (1)	0.126 (1)	0.104 (7)[c]
O(7w)[b]	0.881 (2)	0.043 (2)	−0.048 (1)	0.126 (7)[c]
O(8w)[b]	0.738 (3)	0.414 (2)	0.873 (3)	0.11 (1)[c]
O(9w)[b]	0.924 (3)	0.399 (2)	0.003 (2)	0.12 (1)[c]
O(10w)[b]	0.873 (6)	0.105 (4)	0.041 (4)	0.12 (3)[c]
O(11w)[b]	0.878 (5)	0.472 (3)	0.083 (3)	0.16 (1)[c]
O(12w)[b]	0.669 (3)	0.480 (2)	0.896 (2)	0.11 (1)[c]

[a] Equivalent isotropic U defined as one-third of the trace of the orthogonalized U_{ij} tensor. [b] Water sites O(6w)–O(12w) are partially occupied. Their occupancy factors were modeled as 0.80, 0.64, 0.52, 0.48, 0.20, 0.38, and 0.45, respectively. [c] Atoms O(6w)–O(12w) were refined with isotropic thermal parameters.

Results

Kinetic Studies. The proton magnetic resonance spectroscopy of the bis(pyridoxylideneglycinato)cobaltate(III) anion provides an effective technique for measuring the rates of exchange of the

(7) Cromer, D. T.; Waber, J. T. *International Tables for X-ray Crystallography*; Kynoch: Birmingham, England, 1974; Vol. IV, pp 72–98, 149–150.

(8) Aleksandrov, G. G.; Struchkov, Y. T.; Belkon, Y. N. *Zh. Strukt. Khim.* **1975**, *16*, 875.

(9) Capasso, S.; Giordano, F.; Maltia, C.; Mazzarella, L.; Ripamonti, A. *J. Chem. Soc., Dalton Trans.* **1974**, 2228.

(10) Cutfield, J. F.; Hall, D.; Waters, T. N. *Chem. Commun.* **1967**, 785.

Table III. Summary of the Rate Data for the Reactions Substituting D for H in the Glycyl Methylene Group

	fast reaction		slow reaction	
temp, K	pD range	rate const, L mol^{-1} s^{-1}	pD range	rate const, L mol^{-1} s^{-1}
286	9.64–10.08	35.5	9.64–10.08	6.88
293	8.92–9.82	92.5	8.59–10.61	13.0
304	8.59–9.51	185	9.05–10.45	48.2
314	8.83–9.70	493	9.37–10.38	115

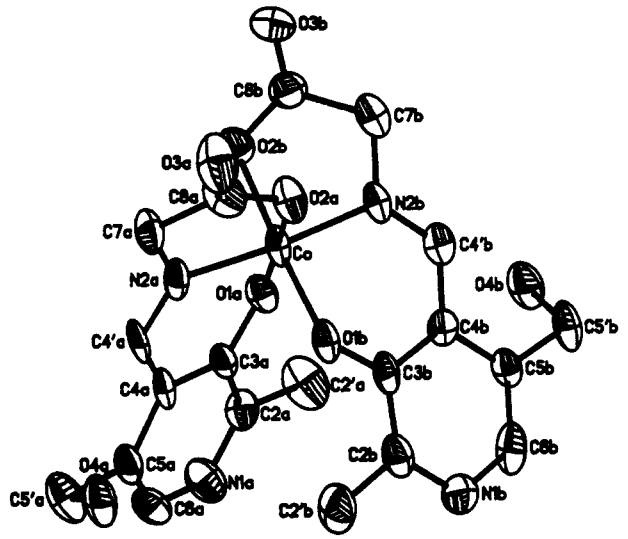

Figure 2. Structure of the bis(pyridoxylideneglycinato)cobaltate(III) anion.

methylene protons of the glycine portion of the ligand. In Figure 1a, trace A is an expansion of the glycine methylene region before any exchange has taken place. It shows this group as an AB pattern with long-range coupling of each resonance to the azomethine proton four bonds away. The long range couplings of the A and B parts are different, showing that the glycine methylene protons have different dihedral angles with the azomethine CH and, therefore, a different dihedral angle with the plane of the pyridine ring.

Figure 1 shows the changes observed in the AB pattern as deuterium exchange progresses. The key feature to be noted is that the high-field portion of the AB pattern disappears more rapidly than the low-field portion. Singlets are clearly visible at intermediate times during the reaction. These singlets correspond to the proton signals of the two monodeuterated glycine methylene signals resulting from substitution of each of the two different glycine methylene protons by a single deuterium. Integration of the glycine methylene region provided the data from which the kinetics in this study were derived. Each of the methylene protons disappeared in a simple first-order process. Correlation coefficients of linear least-squares plots were 0.97 or better. The secondary isotope effect could not be reliably measured as the adjacent proton is replaced by deuterium in the methylene group.

Studies were carried out in carbonate/bicarbonate buffers over a range of pH's. By variation of the total buffer concentration and the pH, it was established that the rate is [OD$^-$] dependent and that the rate law is given by eq 1. Table III contains the

$$\text{rate} = k(\text{complex})\ [\text{OD}^-] \qquad (1)$$

rate constants measured over a range of temperatures. From the data, $\Delta H^* = 74.7$ kJ mol^{-1} and $\Delta S^* = -15$ J mol^{-1} K^{-1} for the more slowly exchanging proton and $\Delta H^* = 59.5$ kJ mol^{-1} and $\Delta S^* = -52$ J mol^{-1} K^{-1} for the more rapidly exchanging proton.

Crystal and Molecular Structure. Suitable crystals for X-ray diffraction were obtained as the tetramethylammonium salt of the bis(pyridoxylideneglycinato)cobaltate(III) anion. The structure of the anion appears in Figure 2; bond lengths and angles are given in Table IV. Poor crystal quality and disorder of the lattice waters and tetramethylammonium ion require that some caution be exercised in interpreting the crystallographic results. In particular, bond distances and angles should be regarded as less accurate than estimated standard deviations might indicate.[11] In spite of its limitations, the crystal structure establishes stereochemical features of the complex that are relevant to the results of kinetics studies.

Table IV. Bond Lengths (Å) and Angles (deg) with Standard Deviations in Parentheses for $[N(CH_3)_4][Co(C_{10}H_{10}N_2O_4)_2]\cdot 4.5H_2O$

bond lengths				av
C(2a)–C(3a)	1.38 (2)	C(2b)–C(3b)	1.40 (2)	1.39
C(2a)–C(2'a)	1.51 (2)	C(2b)–C(2'b)	1.53 (1)	1.52
C(2a)–N(1a)	1.36 (1)	C(2b)–N(1b)	1.35 (2)	1.35
C(3a)–C(4a)	1.41 (1)	C(3b)–C(4b)	1.42 (1)	1.42
C(3a)–O(1a)	1.30 (1)	C(3b)–O(1b)	1.33 (1)	1.32
C(4a)–C(5a)	1.42 (1)	C(4b)–C(5b)	1.42 (2)	1.42
C(4a)–C(4'a)	1.42 (2)	C(4b)–C(4'b)	1.40 (2)	1.41
C(5a)–C(6a)	1.35 (2)	C(5b)–C(6b)	1.36 (2)	1.35
C(5a)–C(5'a)	1.53 (2)	C(5b)–C(5'b)	1.49 (1)	1.51
C(6a)–N(1a)	1.34 (1)	C(6b)–N(1b)	1.36 (1)	1.35
C(4'a)–N(2a)	1.30 (1)	C(4'b)–N(2b)	1.29 (2)	1.30
C(5'a)–O(4a)	1.41 (1)	C(5'b)–O(4b)	1.43 (1)	1.42
C(7a)–C(8a)	1.55 (1)	C*7b)–C(8b)	1.51 (2)	1.53
C(7a)–N(2a)	1.45 (1)	C(7b)–N(2b)	1.46 (1)	1.45
C(8a)–O(2a)	1.27 (1)	C(8b)–O(2b)	1.31 (1)	1.29
C(8a)–O(3a)	1.23 (1)	C(8b)–O(3b)	1.19 (2)	1.21
Co–N(2a)	1.890 (8)	Co–N(2b)	1.877 (7)	1.883
Co–O(1a)	1.901 (6)	Co–O(1b)	1.883 (8)	1.892
Co–O(2a)	1.911 (7)	Co–O(2b)	1.919 (8)	1.915
N(3)–C(11)	1.52 (3)	N(3)–C(12)	1.47 (3)	
N(3)–C(13)	1.49 (3)	N(3)–C(14)	1.47 (3)	
C(3a)–C(2a)–C(2'a)	120 (1)	C(3b)–C(2b)–C(2'b)	120 (1)	120
C(3a)–C(2a)–N(1a)	123 (1)	C(3b)–C(2b)–N(1b)	123 (1)	123
C(2'a)–C(2a)–N(1a)	117 (1)	C(2'b)–C(2b)–N(1b)	116 (1)	117
C(2a)–C(3a)–C(4a)	117 (1)	C(2b)–C(3b)–C(4b)	118 (1)	118
C(2a)–C(3a)–O(1a)	118 (1)	C(2b)–C(3b)–O(1b)	119 (1)	118
C(4a)–C(3a)–O(1a)	125 (1)	C(4b)–C(3b)–O(1b)	123 (1)	124
C(3a)–C(4a)–C(5a)	119 (1)	C(3b)–C(4b)–C(5b)	119 (1)	119
C(3a)–C(4a)–C(4'a)	122 (1)	C(3b)–C(4b)–C(4'b)	122 (1)	122
C(5a)–C(4a)–C(4'a)	120 (1)	C(5b)–C(4b)–C(4'b)	120 (1)	120
C(4a)–C(5a)–C(6a)	118 (1)	C(4b)–C(5b)–C(6b)	118 (1)	118
C(4a)–C(5a)–C(5'a)	121 (1)	C(4b)–C(5b)–C(5'b)	123 (1)	122
C(6a)–C(5a)–C(5'a)	121 (1)	C(6b)–C(5b)–C(5'b)	119 (1)	120
C(5a)–C(6a)–N(1a)	124 (1)	C(5b)–C(6b)–N(1b)	126 (1)	125
C(4a)–C(4'a)–N(2)	124 (1)	C(4b)–C(4'b)–N(2b)	124 (1)	124
C(5a)–C(5'a)–O(4a)	108 (1)	C(5b)–C(5'b)–O(4b)	107 (1)	107
C(8a)–C(7a)–N(2a)	106 (1)	C(8b)–C(7b)–N(2b)	110 (1)	108
C(7a)–C(8a)–O(2a)	117 (1)	C(8b)–C(7b)–O(2b)	113 (1)	115
C(7a)–C(8a)–O(3a)	118 (1)	C(7b)–C(8b)–O(3b)	122 (1)	120
O(2a)–C(8a)–O(3a)	125 (1)	O(2b)–C(8b)–O(3b)	125 (1)	125
C(2a)–N(1a)–C(6a)	118 (1)	C(2b)–N(1b)–C(6b)	117 (1)	117
C(4'a)–N(2a)–C(7a)	123 (1)	C(4'b)–N(2b)–C(7b)	124 (1)	124
Co–N(2a)–C(4'a)	124.4 (8)	Co–N(2b)–C(4'b)	125.2 (7)	125
Co–N(2a)–C(7a)	112.2 (6)	CO–N(2b)–C(7b)	110.3 (7)	111
Co–O(1a)–C(3a)	120.6 (6)	Co–O(1b)–C(3b)	120.7 (6)	121
Co–O(2a)–C(8a)	114.1 (6)	Co–O(2b)–C(8b)	115.3 (7)	115
N(2a)–Co–O(1a)	92.6 (3)	N(2b)–Co–O(1b)	91.9 (3)	92.3
N(2a)–Co–O(2a)	84.8 (3)	N(2b)–Co–O(2b)	85.1 (3)	85.0
O(1a)–Co–O(2a)	177.3 (3)	O(1b)–Co–O(2b)	176.9 (3)	177.1
O(1a)–Co–N(2b)	92.6 (3)	O(1b)–Co–N(2a)	91.6 (3)	92.1
O(2a)–Co–N(2b)	90.0 (3)	O(2b)–Co–N(2a)	91.4 (3)	90.7
O(1a)–Co–O(2b)	91.4 (3)	O(1b)–Co–O(2a)	90.9 (3)	91.2
N(2a)–Co–N(2b)	173.7 (4)	O(1a)–Co–O(1b)	89.1 (3)	
O(2a)–Co–O(2b)	88.8 (3)	C(11)–N(3)–C(12)	111 (2)	
C(11)–N(3)–C(13)	109 (2)	C(11)–N(3)–C(14)	108 (2)	
C(12)–N(3)–C(13)	110 (2)	C(12)–N(3)–C(14)	109 (2)	
C(13)–N(3)–C(14)	110 (2)			

(11) During the course of structure refinement, two other models were tried for the lattice water sites. These were judged less satisfactory than the chosen model, since they led to higher R values and larger standard deviations for all refined parameters. However, the results obtained with the alternative models indicate the effects of disorder among lattice water sites on the accuracy and reliability of refined parameters for the cobalt complex. Results obtained when the seven partially occupied water sites were replaced by four fully occupied sites differed from those obtained by the chosen model by less than 2esd for individual parameters. With a more extreme model, where none of the partially occupied water sites were included, the largest difference was 4.5esd for the y/b coordinate of C(2'b). The dihedral angles and interproton distances reported in the Discussion reflect the ranges obtained with these alternative models for the lattice waters.

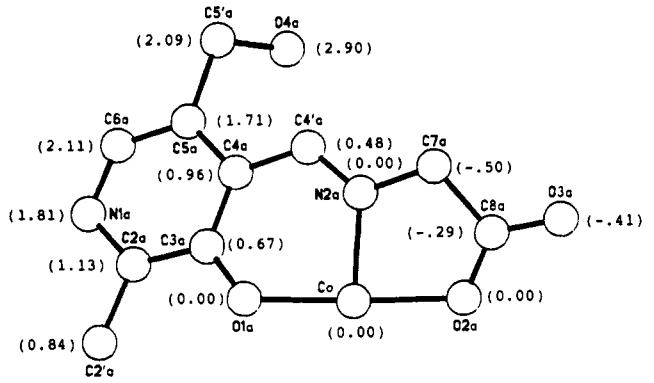

Figure 3. Projection of ligands on the CoO(1)O(2)N(2) plane for the bis(pyridoxylideneglycinato)cobaltate(III) anion. Numbers in parentheses are the displacement (in angstroms) of atoms above or below this plane.

It is observed that the chelate rings are not planar. Figure 3 presents a particularly useful representation of one of the ligands in the complex. A plane has been passed through the cobalt ion and through the oxygen and nitrogen atoms bound to it. The numbers in parentheses next to each atom in the ligand give its displacement in angstroms from this plane. Reference to Figure 2 shows that the distortion of the chelate ring is such that the glycine methylene carbon atom of one ligand is on the opposite side of the ligand plane from the aromatic ring 2-CH_3 group of the other ligand. It also shows that the azomethine carbon atom is on the opposite side of the plane from the methylene carbon atom of the glycine moiety of a given ligand.

Discussion

In the crystalline state, the title anion is distorted so that the two methylene protons of the glycine moiety have different dihedral angles with the plane of the π system. While X-ray diffraction data are not adequate to determine proton positions, the location of the methylene carbon atom is strong evidence. Reference to Table IV shows that the bond angles at the azomethine carbon and at the glycine α-carbon atom are nearly those expected for sp^2 and sp^3 carbon atoms, respectively. Assuming the carbon–hydrogen bond angles and bond lengths to be ideal, one may calculate the dihedral angles between the glycyl carbon–hydrogen bond and the azomethine C–H. One may also calculate interproton distances. The dihedral angles are -29 ± 2 and $89 \pm 2°$. The distances are 2.39 ± 0.03 and 3.04 ± 0.03 Å.[11]

In solution, NMR spectroscopy provides further support for the methylene protons having different geometric relationships with the azomethine π system. Nuclear Overhauser enhancements are observed for the glycyl methylene resonances when the azomethine proton is irradiated. The enhancements are too small to be measured accurately, but they are significantly larger for the downfield part of the glycyl AB resonance (2%) than for the upfield proton (1%). The pseudoallylic four-bond coupling between the azomethine hydrogen and the methylene protons is also different (1.33 and 2.26 Hz, respectively). Since couplings increase as protons approach the dihedrally perpendicular angle of 90°,[12] we assign the upfield NMR signal to the proton in the position predicted to be eliminated most readily by an electron shift such as that shown in II. As demonstrated in Figure 1, the upfield proton is the one most readily exchanged for deuterium in our system.

Barfield, Spear, and Sternhell have reviewed the geometric dependence of a pseudoallylic four-bond proton–proton coupling constant on the dihedral angle.[12] The coupling constant is the sum of terms of opposite signs involving transmission through σ and π orbitals. Theory and experiment agree reasonably well, and these authors provide figures showing the angular dependence of coupling constant on dihedral angle. Azomethine systems like the one we have studied have not been analyzed in detail; however, we have shown the importance of substituent electronic effects upon the pseudoallylic coupling constants for a series of 12 cobalt(III) Schiff base complexes.[13] The combination of these data and Barfield, Spear, and Sternhell's equations predict dihedral angles of about −47 and +78° for our system. While these values are close to those deduced from X-ray crystallography, any simple scaling of the Barfield, Spear, and Sternhell figures predicts a smaller angle that is somewhat too large and a larger angle that is too small in our system. Since there are two terms of opposite signs in the expression for the coupling constant, it is possible that the shape of the curve is different for azomethine complexes than it is for other systems. Another possibility is that the chelate ring involving the methylene carbon atom and/or the ring involving the azomethine proton is undergoing an inversion rapid on the NMR time scale. If this were the case, the dihedral angles observed from the NMR experiment would be averages and would be different from those determined by crystallography. The data at hand do not permit the resolution of these issues, but they do show clearly that the proton with the greatest dihedral angle to the π system exchanges most rapidly.

Stereoselective proton abstractions have been studied in complexes of different glycyl derivatives. A chiral complex of a tridentate diprolyl ligand and the 2-picolinoylamide of glycine shows an 8-fold difference in exchange rate for the glycine protons.[14] Cobalt(III) complexes of an *N*-arylglycine show as much as a 4-fold rate difference.[15,16] Steric effects have been invoked to explain different rates for proton exchange. These steric effects differentially impede the approach of OH^- toward either proton of the methylene group or they differentially impede the approach of H_2O to reprotonate one side or the other of the carbanion intermediate that is formed. Bosnich has pointed out that these two processes are identical under the principle of microscopic reversibility.[14]

Steric effects provide no obvious explanation for the stereoselectivity we observe. In the complex bis((3-methylsalicylidene)glycinato)cobaltate(III), glycine proton exchange rates have been studied. The 3-methyl group is located at the same place on the salicyl aromatic ring as is the 2-CH_3 group in the pyridoxal systems. Different rates of exchange are observed for the glycine protons. It was observed that the 3-CH_3 group of one ligand was closer to the slowly exchanging proton of the other ligand. It was suggested that this methyl group might impede hydroxide ion abstraction of that proton, in the fashion described above for the glyclyl complexes. In our system the 2-CH_3 group of one ligand makes the closest approach to the slowly exchanging proton of the other ligand. However, the shortest distance between a methyl proton and the slowly exchanging methylene proton is 4.7 Å. This would seem to leave adequate room for the approach of a hydroxide ion. No other obvious structural features impede the approach of OH^- toward this glycyl proton. In our system, the more rapidly exchanging proton is more hindered. It is 2.86 Å from the carboxylate oxygen of the other ligand (O(2)) and may not be as accessible to hydroxide ion in solution as is the more slowly exchanging proton.

For the more rapidly exchanging proton ΔH^* is less positive than for the more slowly exchanging proton. On the other hand, ΔS^* is much more negative for the rapidly exchanging proton than for the slowly exchanging proton. The difference in the activation entropies would seem to argue against steric explanations for stereoselectivity. One would think that if steric effects impeded the approach of OH^-, then ΔS^* would be more negative for the more slowly exchanging proton. The values of ΔS^* we observe would indicate that OH^- must approach the more rapidly ex-

(12) Barfield, M.; Spear, R. J.; Sternhell, S. *Chem. Rev.* **1976**, *76*, 93.

(13) Fischer, J. R.; Fischer, R.; Abbott, E. H. *Inorg. Chem.* **1990**, *29*, 1682.

(14) Dokuzovic, Z.; Roberts, N. K.; Sawyer, J. F.; Whelan, J.; Bosnich, B. *J. Am. Chem. Soc.* **1986**, *108*, 2034–2039.

(15) Golding, B. T.; Gainsford, G. T.; Aerlt, A. J.; Sargeson, A. M. *Tetrahedron* **1976**, *32*, 389–397.

(16) Golding, B. T.; Ioannou, P. V.; Sellers, P. J. *Inorg. Chim. Acta* **1981**, *56*, 95–98.

(17) Belokon, Y. N.; Melikyan, A. S.; Salel'eva, T. F.; Bakhmutov, V. I.; Vitt, S. V.; Belikov, V. M. *Tetrahedron* **1980**, *36*, 2327–2335.

changing proton by a more restricted trajectory perhaps because of the steric effects described above. The activation enthalpies we observe and the electronic explanation we offer for the different rate of exchange of the glycine protons is consistent with a recent neutron diffraction study of a related system.[18] In the (salicylideneglycinato)copper(II) complex, it was observed that the glycine chelate ring was distorted and the proton had dihedral angles of -32.9 and 77.9° with the plane of the salicyl aromatic ring. It was observed that the proton at the higher angle had a C-H bond length more than 3σ longer than the proton at the lower angle. The longer bond length is consistent with a reduced ΔH^* for exchange, such as we observe.

A concluding point concerns the magnitude of ΔH^* for the more rapidly exchanging proton. In an enzyme, the base is part of the active site. This enables ΔS^* to be close to zero. If ΔS^* were zero in our system, one may calculate that the rate constant would be 300 L mol^{-1} s^{-1}. This approaches the rates observed for enzyme-catalyzed reactions.

Acknowledgment. We gratefully acknowledge support of this work at Montana State University by Grant CHE 7826160 from the National Science Foundation, Grant AM-21669 from the National Institutes of Health, and Cooperative Agreement CR809478 from the Environmental Research Laboratory—Duluth, Environmental Protection Agency. Work at Western New Mexico University was supported by a grant from the Research Corp.

Supplementary Material Available: Listings of crystal data and structure refinement parameters, least-squares planes, and anisotropic thermal parameters (2 pages); a listing of observed and calculated structure factors (8 pages). Ordering information is given on any current masthead page.

(18) Bkouche-Waksman, I.; Barke, J. M.; Kvick, A. *Acta Crystallogr., Sect. B* **1988**, *B44*, 595.

Contribution from the Departamento de Química Inorgánica, Universidad de Granada, 18071 Granada, Spain, Departamento de Química, Universidad de Barcelona, Plaza Imperial Tarraco, 1, 43005 Tarragona, Spain, and Laboratoire de Chimie Analitique II, Université Claude Bernard, 69622 Villeurbanne, France

A New Type of Divalent Metal Nucleosidate Complex: Crystal Structure of *trans*-Tetraaquobis(xanthosinato)zinc(II) Dihydrate

Miguel Quirós,[†] Juan M. Salas,*[,†] M. Purificación Sánchez,[†] Juan R. Alabart,[‡] and René Faure[§]

Received May 14, 1990

Several complexes of divalent transition metals with the anionic form of the purine nucleosides guanosine, inosine, and xanthosine have been isolated and characterized by thermal and spectroscopic techniques and magnetic measurements. The complexes have the general formula $[M(Nuc)_2(H_2O)_4]\cdot nH_2O$ (except the cadmium complex, which has the formula $[Cd(Xao)_2(H_2O)_2]\cdot 5H_2O$). The coordinated and uncoordinated water molecules are clearly identified by TG and DSC diagrams. The octahedral coordination for Mn, Co, Ni, and Cu is supported by the magnetic measurements. NMR data for cadmium xanthosinate indicate coordination through N3. The crystal structure of *trans*-$[Zn(Xao)_2(H_2O)_4]\cdot 2H_2O$ has been solved by X-ray diffraction. This is the first time that the structure of a xanthosine complex has been described and also the first description of the structure of a purine nucleoside complex with a divalent metal of the first transition series. The N7-coordinated xanthosinate is located at the apex of the octahedral complex. The structure reveals an interesting hydrogen-bonding scheme and unusual sugar conformations.

Introduction

The interaction of metal ions with nucleic acid derivatives is of considerable interest due to the biological importance of such compounds. The research carried out can be classified according to the complexity of the nucleic acid fragments, i.e. complexes with heterocyclic bases, nucleosides, nucleotides, polynucleotides, and nucleic acids themselves. The first case (bases) and the third case (nucleotides) have been studied much more than the second one (nucleosides), probably due to the fact that nucleoside complexes are generally obtained in the form of polymeric and colloidal species and are difficult to crystallize. More than 80 references to crystal structures of nucleotide–metal complexes exist compared to only 14 for pyrimidine and purine nucleoside–metal complexes: $([Pt(en)(Guo)_2]Cl_{1.5}I_{0.5}\cdot 2H_2O$,[1] $[Co(acac)_2(NO_2)(dAdo)]$,[2] *cis*-$[Pt(NH_3)_2(Guo)_2]Cl_{1.5}(ClO_4)_{0.5}\cdot 7H_2O$,[3] *catena*-$[Hg(\mu\text{-}Cl)Cl(Guo)]$,[4] $[Pt(dien)(Ino)](NO_3)_2$,[5] $[Pt(dien)(Guo)](ClO_4)_2$,[6] $[Pd(dien)(Guo)](ClO_4)_2$,[7] $[(CH_3Hg)_2(\mu\text{-Ino-}N1,N7)](ClO_4)$,[8] $[PtCl(en)(AraCyt)]Cl$,[9] $[CH_3Hg(Thd)]$,[10] $[Cu(GlyGly)(Cyd)]$,[11] *catena*-$[Hg(\mu Br)Br(Guo)]$,[12] *trans*-$[Pd(Ino)_2Cl_2]\cdot 5H_2O$, and *trans*-$[Pd(Ino)_2Br_2]\cdot 3H_2O$[13] where Guo = guanosine, dAdo = 2′-deoxyadenosine, Ino = inosine, AraCyt = 9-β-D-arabinofuranosylcytosine, Thd = thymidine, Cyd = cytidine, en = ethylenediamine, acac = acetylacetonato, dien = diethylenetriamine, and GlyGly = glycylglycinato).

Work on solid-phase studies of nucleoside–metal complexes has usually been focused on Pt(II),[1,3,5,6,14-18] Pd(II),[7,13,19,20] and Hg-

* To whom correspondence should be addressed.
† Universidad de Granada.
‡ Universidad de Barcelona.
§ Université Claude Bernard.

(1) Gellert, R. W.; Bau, R. *J. Am. Chem. Soc.* **1975**, *97*, 7379.
(2) Sorrel, T.; Epps, C. A.; Kistenmacher, T. J.; Marzilli, L. G. *J. Am. Chem. Soc.* **1977**, *99*, 2173.
(3) Cramer, R. E.; Dahlstrom, P. L.; Seu, M. J. T.; Norton, T.; Kashiwagi, M. *Inorg. Chem.* **1980**, *19*, 148.
(4) Authier-Martin, M.; Hubert, J.; Rivest, R.; Beauchamp, A. L. *Acta Crystallogr.* **1978**, *B34*, 273.
(5) Melanson, R.; Rochon, F. D. *Acta Crystallogr.* **1978**, *B34*, 3594.
(6) Melanson, R.; Rochon, F. D. *Can. J. Chem.* **1979**, *57*, 57.
(7) Rochon, F. D.; Kong, P. C.; Coulombe, B.; Melanson, R. *Can. J. Chem.* **1980**, *58*, 381.
(8) Bélanger-Gariepy, F.; Beauchamp, A. L. *Cryst. Struct. Commun.* **1982**, *11*, 991.
(9) Neidle, S.; Taylor, G. L.; Robins, A. B. *Acta Crystallogr.* **1978**, *B34*, 1838.
(10) Guay, F.; Beauchamp, A. L. *Can. J. Chem.* **1985**, *63*, 3456.
(11) Szalda, D. J.; Marzilli, L. G.; Kistenmacher, T. J. *Biochem. Biophys. Res. Commun.* **1975**, *63*, 601.
(12) Quirós, M.; Salas, J. M.; Sánchez, M. P.; Faure, R. *An. Quím.* **1990**, *86*, 518.
(13) Quirós, M.; Salas, J. M.; Sánchez, M. P.; Solans, X.; Beauchamp, A. L. *Can. J. Chem.*, submitted for publication.
(14) Hadjiliadis, N.; Theophanides, T. *Inorg. Chim. Acta* **1976**, *16*, 67.
(15) Hadjiliadis, N.; Theophanides, T. *Inorg. Chim. Acta* **1976**, *16*, 77.
(16) Kong, P. C.; Theophanides, T. *Inorg. Chem.* **1974**, *13*, 1167.
(17) Gullotti, M.; Pacchioni, G.; Pasini, A.; Ugo, R. *Inorg. Chem.* **1982**, *21*, 2006.
(18) Kasselouri, S.; Garoufis, A.; Hadjiliadis, N. *Inorg. Chim. Acta* **1987**, *135*, L23.

0020-1669/91/1330-2916$02.50/0